Journal of Applied Pharmaceutical Research
Volume 14 Issue 4, Year of Publication 2026, Page 151 – 168
DOI: https://doi.org/10.69857/joapr.v14i4.2180

Check for updates

Research Article

JOURNAL OF APPLIED PHARMACEUTICAL RESEARCH | JOAPR
www.japtronline.com *ISSN: 2348 – 0335*

BILAYER MUCOADHESIVE INTRAUTERINE DELIVERY PLATFORM FOR SUSTAINED PLATELET-DERIVED EXTRACELLULAR VESICLE RELEASE TO PROMOTE ENDOMETRIAL REGENERATION AND IMPROVE IMPLANTATION OUTCOMES

Rajaganapathy Kaliyaperumal*, Srinivasan R, Kalaivanan Seeni, Vignesh Sekar

Article Information
Received: 7th March 2026
Revised: 22nd June 2026
Accepted: 10th July 2026
Published: 31st July 2026

Keywords
Extracellular vesicles, Endometrial regeneration, Mucoadhesive delivery, Bilayer system, Implantation, Platelet-rich plasma

ABSTRACT
Background: Endometrial dysfunction remains a major cause of implantation failure and infertility. Extracellular vesicles (EVs) derived from platelet-rich plasma have shown regenerative potential; however, their clinical application is limited by rapid clearance and poor retention within the uterine cavity. **Methodology:** A bilayer mucoadhesive intrauterine delivery platform was developed for sustained release of platelet-derived extracellular vesicles. The bilayer system consisted of a mucoadhesive EV-loaded layer and a protective anti-adhesion layer. Physicochemical characterization, EV release kinetics, and mucoadhesion properties were evaluated. In vitro studies of wound healing, cell proliferation, and gene expression were performed. In vivo efficacy was assessed through histological evaluation of endometrial thickness and implantation outcomes. **Results and Discussion:** The bilayer platform demonstrated sustained extracellular vesicle release for up to 120 h with minimal initial burst release. Enhanced cell migration and proliferation, along with upregulation of endometrial receptivity markers including LIF, HOXA10, Integrin αV/β3, and IGFBP1, were observed. In vivo studies revealed significant improvement in endometrial thickness and implantation sites in the EV-Pad group compared to controls. The sustained release of EVs improved endometrial regeneration and enhanced implantation potential. The bilayer design demonstrated improved local retention characteristics and enhanced regenerative responses compared with free EV administration under experimental conditions. **Conclusion:** The developed bilayer mucoadhesive intrauterine delivery system provides a promising strategy for sustained EV delivery and improved endometrial regeneration, supporting its potential as a preclinical platform for sustained intrauterine regenerative delivery.

INTRODUCTION

Implantation failure and inadequate endometrial receptivity remain major limiting factors in assisted reproductive technologies and infertility management, contributing substantially to unsuccessful pregnancy outcomes even in cases where embryo quality is optimal [1-4]. A structurally and

*Faculty of Pharmacy, Bharath Institute of Higher Education and Research, Selaiyur, Chennai- 600073, Tamil Nadu, India

***For Correspondence:** **rajaganapathy.pharmacy@bharathuniv.ac.in**

functionally competent endometrium is essential for successful embryo attachment, invasion, and placental development [5-7]. However, conditions such as thin endometrium, chronic inflammation, impaired angiogenesis, and insufficient stromal remodeling can disrupt the synchronized molecular events required during the implantation window. Conventional therapeutic approaches, including hormonal stimulation, platelet-rich plasma infusion, and growth factor supplementation, have demonstrated variable clinical success and often suffer from rapid clearance, poor local retention, and inconsistent biological activity. These challenges highlight the urgent need for localized regenerative strategies that provide sustained biochemical signaling while maintaining tissue compatibility and procedural safety [8,9].

Extracellular vesicles derived from platelets have recently emerged as promising biologically active nanoscale mediators capable of modulating cellular proliferation, angiogenesis, immune regulation, and tissue regeneration through their cargo of growth factors, cytokines, proteins, and regulatory nucleic acids [10-15]. Unlike direct cell-based therapies, extracellular vesicles offer improved biosafety, reduced immunogenicity, and enhanced stability while preserving essential paracrine signaling functions [16-18]. Increasing evidence suggests that vesicle-mediated signaling can enhance endometrial repair, promote vascular remodeling & activate implantation-associated molecular pathways [19-22]. Nevertheless, the clinical translation of extracellular vesicle therapy for intrauterine applications remains limited due to critical delivery challenges, including rapid dispersion in uterine fluid, insufficient mucosal adherence, uncontrolled dosing, and the lack of reliable sustained-release platforms that synchronize vesicle availability with the implantation timeline [23,24]. Biomaterial-assisted delivery systems have been explored to improve localized therapeutic retention in mucosal tissues, with mucoadhesive polymers such as chitosan and hyaluronic acid demonstrating strong potential due to their biocompatibility, hydration properties, and capacity to form stable biointeractive matrices [25-27]. Thiolated derivatives of chitosan further enhance mucosal adhesion through covalent bonding with mucin glycoproteins, thereby improving residence time in dynamic physiological environments [28,29]. At the same time, polyethylene glycol-based materials have been widely used as anti-adhesion surfaces due to their hydrophilicity and resistance to nonspecific protein binding. While these materials have individually shown promise in biomedical applications, their combined use in a structurally engineered bilayer intrauterine system specifically designed for controlled extracellular vesicle delivery has not been comprehensively investigated [30,31]. Existing intrauterine therapeutic approaches largely rely on fluid instillation or injectable formulations, which lack structural stability, controlled spatial positioning, and retrievability, thereby limiting reproducibility and clinical control [32,33].

The present work addresses this unmet need by proposing a structurally differentiated bilayer intrauterine delivery platform that integrates a thiolated chitosan–hyaluronic acid mucoadhesive, endometrium-facing layer for sustained vesicle retention, with a polyethylene glycol-based luminal anti-adhesion surface to prevent tissue fusion and enable atraumatic removal. This design aims to provide controlled vesicle release synchronized with the implantation window while simultaneously ensuring mechanical stability, tissue compatibility, and procedural practicality. The integration of extracellular vesicle stabilization strategies, controlled low-temp. fabrication & mechanical retrieval features represents a novel engineering approach intended to provide foundational preclinical evidence supporting further development of biomaterial-guided intrauterine vesicle delivery systems. Accordingly, the present study aimed to develop and evaluate a bilayer mucoadhesive intrauterine delivery system for the sustained, localized administration of platelet-derived extracellular vesicles to enhance endometrial regeneration and implantation outcomes. The study systematically investigated vesicle isolation and quality validation, bilayer polymeric delivery platform fabrication, physicochemical and mechanical characterization, controlled vesicle release kinetics, preservation of biological functionality following incorporation, and the regenerative effects of sustained vesicle exposure in cellular and in vivo implantation impairment models. Through this integrated experimental framework, the work seeks to provide proof of concept demonstrating the feasibility, biological effectiveness, and translational potential of biomaterial-guided extracellular vesicle delivery as a next-generation therapeutic strategy to improve uterine receptivity and reproductive success [34].

MATERIALS AND METHODS

Materials

Pharmaceutical-grade chitosan (degree of deacetylation 75–85%) and hyaluronic acid (molecular weight 100–300 kDa) were used as primary polymers for fabrication of the mucoadhesive

endometrium-facing layer. Thioglycolic acid was employed for thiolation of chitosan to enhance covalent mucoadhesive interaction with mucin glycoproteins. Polyethylene glycol (PEG 4000 or PEG diacrylate) served as the anti-adhesion polymer for the lumen-facing layer. Trehalose and mannitol were used as extracellular vesicle stabilizers during loading and drying processes. Platelet concentrates obtained from screened donor blood served as the source of platelet-derived extracellular vesicles (PEVs). Phosphate-buffered saline (PBS, pH 7.2) and acetate buffer (pH 5.5) were used for polymer preparation and washing procedures. Analytical reagents included ELISA kits for receptivity markers, endotoxin detection kits based on Limulus Amebocyte Lysate assay, and standard microbiological sterility testing media. All reagents were analytical or cell-culture grade and used without further purification.

Isolation and Standardization of Platelet-Derived Extracellular Vesicles

Platelet concentrates obtained from screened healthy donor blood were processed within 4 h of collection under sterile conditions. Platelet concentrates were obtained from six healthy voluntary donors (age range: 22–35 years) following institutional ethical approval and informed consent procedures. Donors were screened to exclude systemic inflammatory disorders, infectious diseases, hematological abnormalities, hormonal therapy, smoking history, chronic medication use, and recent administration of non-steroidal anti-inflammatory drugs within 14 days before blood donation. Platelet concentrates were prepared using a standardized double-spin platelet-rich plasma protocol under blood bank processing conditions. To minimize donor-dependent biological variability and improve batch reproducibility, equal volumes of platelet concentrate from three compatible donors were pooled to generate a single EV isolation batch. Independent EV batches were prepared from two separate donor pools and processed under identical isolation conditions. Inter-donor batch variability was assessed by comparing extracellular vesicle particle size distribution, particle concentration, zeta potential, protein-to-particle ratio, and expression levels of EV markers CD9, CD63, and CD81 across independent pooled batches. Variability between batches remained within an acceptable coefficient of variation threshold (<15%), indicating reproducible extracellular vesicle production and consistent physicochemical characteristics across donor pools. Functional batch consistency was further confirmed by in vitro endometrial cell migration assays before inclusion in biological experiments.

Initial removal of intact platelets and cellular debris was performed by sequential differential centrifugation using a refrigerated high-speed centrifuge equipped with a fixed-angle rotor (Beckman Coulter Avanti J-26XP, JA-25.50 rotor). Samples were first centrifuged at 300 × g for 10 min at 4 °C, then at 2,000 × g for 20 min at 4 °C to remove residual cells and large debris. The resulting supernatant was further centrifuged at 10,000 ×g for 30 min at 4 °C to remove larger microvesicles and apoptotic bodies [35,36].

The clarified supernatant was subsequently purified using size-exclusion chromatography (SEC) performed on qEVoriginal 70 nm columns (Izon Science, New Zealand; column dimensions: 10 mm × 300 mm) pre-equilibrated with sterile phosphate-buffered saline (PBS, pH 7.2). Fractions 7–10, corresponding to extracellular vesicle-rich eluates, were collected according to the manufacturer's specifications and pooled only when nanoparticle tracking analysis confirmed particle concentrations above 1×10^8 particles/mL with particle diameters predominantly between 50–200 nm [36]. The pooled EV fractions were concentrated using Amicon Ultra-15 centrifugal ultrafiltration units (100 kDa molecular weight cut-off, MilliporeSigma, USA) at 4,000 ×g for 20 min at 4 °C. Concentrated vesicle preparations were sterile-filtered through 0.22 μm syringe filters and stored at −80 °C in sterile PBS supplemented with 5% trehalose until further use. Repeated freeze–thaw cycles were avoided, and all preparations were used within 30 days of isolation [37].

Particle size distribution and concentration were determined using nanoparticle tracking analysis (NanoSight NS300, Malvern Instruments, UK) [37]. Only vesicle preparations demonstrating mean particle diameters between 50 and 200 nm, polydispersity within acceptable limits, and concentrations within the predefined therapeutic range were accepted for further study. Protein contamination was assessed using protein-to-particle ratio analysis based on bicinchoninic acid assay measurements. Vesicle identity was confirmed through expression analysis of canonical extracellular vesicle markers CD9, CD63, and CD81 using Western blotting and flow cytometry [38,39]. Representative nanoparticle tracking analysis (NTA) size distribution plots were generated for all accepted EV batches to confirm narrow, nanoscale particle size distributions with minimal aggregation [39]. Protein contamination was quantitatively assessed by determining the protein-to-particle ratio using a bicinchoninic acid protein assay, normalized to the

nanoparticle concentration obtained from NTA analysis. Preparations demonstrating excessive soluble protein contamination were excluded from further studies. Extracellular vesicle loading efficiency within the mucoadhesive polymer matrix was determined indirectly by measuring the number of non-entrapped vesicles in the supernatant after loading and calculating the percentage of vesicles incorporated. The optimized bilayer formulation demonstrated EV loading efficiencies exceeding 82%, indicating effective entrapment of vesicles within the polymeric matrix. Representative characterization data, including NTA plots, TEM micrographs with scale bars, and purity marker analyses, are presented in Figure 1.

Morphological characterization was further performed using transmission electron microscopy (TEM), which revealed spherical, membrane-bound vesicles with intact bilayer structures and diameters consistent with extracellular vesicles. TEM images were acquired at appropriate magnifications with calibrated 100 nm scale bars for structural validation. In addition to positive EV markers, the purity assessment included evaluation of negative contamination markers, including calnexin and GM130, to exclude cellular organelle contamination and confirm preparation purity in accordance with current extracellular vesicle characterization recommendations [39]. Endotoxin levels were quantified using a Limulus Amebocyte Lysate assay and required to remain below 0.5 EU/mL [40]. Sterility testing was performed by incubating samples in aerobic and anaerobic culture media for 14 days under pharmacopeial sterility-testing conditions. Functional potency was evaluated using in vitro migration assays with human endometrial cells, and only batches that produced≥20% enhancement in migration relative to untreated controls were accepted for biological experiments.

Preparation of Thiolated Chitosan–Hyaluronic Acid Mucoadhesive Polymer

Chitosan was dissolved at a concentration of 2% (w/v) in 1% (v/v) aqueous acetic acid solution under continuous magnetic stirring for 12 h at room temperature until complete hydration was achieved. Hyaluronic acid was separately dissolved at 1% (w/v) in sterile phosphate-buffered saline (PBS; pH 7.2). Thiolation of chitosan was performed by carbodiimide-mediated coupling using thioglycolic acid as the thiol donor. Briefly, thioglycolic acid (0.5% w/v) was activated using 1-ethyl-3-(3-dimethylaminopropyl) carbodiimide hydrochloride (EDC; 50 mM) and N-hydroxysuccinimide (NHS; 25 mM) under pH-adjusted conditions (pH 5.5 ± 0.2). The activated thioglycolic acid solution was gradually added to the chitosan solution and allowed to react for 6 h under continuous stirring at ambient temperature [41-43]. The resulting thiolated chitosan was purified by dialysis against deionized water using a 12–14 kDa molecular weight cut-off membrane for 48 h with periodic water replacement, followed by lyophilization. The degree of thiol substitution within the modified chitosan was quantified using Ellman's reagent assay. It was determined to be approximately 312 ± 18 µmol thiol groups per gram of polymer, indicating successful thiolation within the target mucoadhesive range [41-43]. The overall thiolation reaction yield, after purification and lyophilization, was approximately 78 ± 4%.

Structural confirmation of thiolated chitosan was performed using Fourier-transform infrared spectroscopy (FTIR), which demonstrated characteristic absorption bands corresponding to thiol-associated functional groups and amide bond formation. Additional characterization using proton nuclear magnetic resonance (1H-NMR) spectroscopy confirmed successful conjugation of thioglycolic acid onto the chitosan backbone through the appearance of characteristic thiolated side-chain proton signals. Elemental sulfur analysis further verified incorporation of sulfur-containing functional groups following thiolation. The physicochemical stability of the thiolated polymer was evaluated during storage at 4 °C under desiccated conditions for 3 months. No significant reduction in free thiol content, polymer viscosity, or mucoadhesive performance was observed during the stability assessment period, indicating acceptable structural stability of the modified polymer system for subsequent formulation processing and biological application. For fabrication of the mucoadhesive layer, thiolated chitosan and hyaluronic acid solutions were mixed at a 2:1 polymer ratio under sterile conditions to obtain a homogeneous viscous casting solution with a final polymer concentration of 3% (w/v). The final pH of the casting solution was adjusted to 5.8–6.0 to optimize polymer stability and mucoadhesive performance.

FABRICATION OF BILAYER MUCOADHESIVE EV DELIVERY PAD

Formation of Endometrium-Facing Mucoadhesive Layer

Approximately 5 mL of the mucoadhesive polymer casting solution was poured into sterile silicone molds (diameter: 35 mm) placed on a leveled casting surface. Film thickness was

controlled using an adjustable calibrated film applicator set to 400 µm. Partial solvent evaporation was performed under controlled environmental conditions (25 ± 2 °C; relative humidity 40 ± 5%) for 4 h until a semi-solid gel-like consistency suitable for extracellular vesicle incorporation was achieved.

Extracellular Vesicle Loading and Stabilization

Purified platelet-derived extracellular vesicles were suspended in sterile PBS containing 5% trehalose and 2% mannitol as cryo- and lyoprotective stabilizers. The EV suspension was uniformly distributed over the partially dried mucoadhesive layer at a loading density of approximately 1×10^9 particles per pad and allowed to equilibrate for 30 min at 4 °C to facilitate homogeneous diffusion throughout the polymer matrix.

Formation of Anti-Adhesion Luminal Layer

The anti-adhesion layer was prepared using polyethylene glycol diacrylate (PEGDA; 10% w/v) dissolved in sterile deionized water containing 0.05% (w/v) Irgacure 2959 photoinitiator. Approximately 3 mL of the PEG solution was carefully cast over the EV-loaded mucoadhesive layer to generate the bilayer structure. Bilayer bonding was achieved through interfacial polymer entanglement followed by mild ultraviolet crosslinking (365 nm, 5 mW/cm²) for 60 s to stabilize the luminal PEG layer without compromising extracellular vesicle bioactivity [44].

Controlled drying of the completed bilayer films was subsequently performed for 18 h at 25 °C under humidity-controlled conditions (relative humidity <40%). Fully dried films were carefully removed from molds and cut into intrauterine pads measuring approximately 1.0–1.5 cm in length. Final pad thickness was verified using a calibrated digital micrometer and maintained within the predefined range of 400–450µm. A sterile medical-grade polypropylene retrieval filament was incorporated during final assembly to facilitate atraumatic intrauterine removal following therapeutic application.

Physicochemical Characterization of Bilayer EV Pads

Film thickness was measured at multiple positions using a calibrated digital micrometer to ensure uniformity. Swelling behavior was determined by incubating pads in simulated uterine fluid at physiological temperature and calculating percentage mass gain [45,46]. Mucoadhesive strength was quantified using a texture analyzer with mucin-coated substrates, measuring the detachment force required to separate the film from the substrate. Extracellular vesicle release kinetics were evaluated by incubating bilayer pads in simulated uterine fluid (pH 7.0 ± 0.2) at 37 ± 0.5 °C under gentle orbital agitation (50 rpm). Samples were collected at predefined intervals extending from 0.5 h to 120 h (0.5, 1, 2, 4, 8, 12, 24, 48, 72, 96, and 120 h), and released extracellular vesicles were quantified using nanoparticle tracking analysis and EV-specific ELISA assays. Cumulative percentage release, initial burst fraction, and sustained release behavior were calculated from independent experiments. Release kinetics were mathematically modeled using zero-order, first-order, Higuchi, and Korsmeyer–Peppas equations to determine the dominant release mechanism and diffusion behavior of the polymeric delivery matrix [45,46]. Bioactivity retention following fabrication was assessed using dose-normalized comparative functional assays between freshly isolated extracellular vesicles and pad-released extracellular vesicles standardized to equivalent particle concentrations (1×10^8 particles/mL). All biological outcome assessments were performed under blinded analysis conditions during migration quantification and image-based cellular evaluations. Human endometrial epithelial and stromal cells were separately exposed to freshly isolated EVs, pad-released EVs, blank polymer pad extracts, polymer plus stabilizer controls, and untreated media controls. Additional controls containing trehalose/mannitol stabilizer solution without extracellular vesicles were included to exclude excipient-mediated biological effects. Cellular proliferation, migration, and angiogenic signaling responses were subsequently quantified using standardized wound-healing, viability, and endothelial tube-formation assays. EV-specific biological activity was confirmed only when pad-released vesicle groups demonstrated significantly greater responses than all non-EV control formulations under equivalent experimental conditions [47]. Potential local and systemic safety was evaluated through histological irritation scoring, inflammatory cytokine analysis, fibrosis assessment, adhesion scoring, serum biochemical profiling, and preliminary biodistribution screening. Uterine tissues were examined for epithelial disruption, edema, inflammatory infiltration, fibrosis, and intrauterine adhesion formation using hematoxylin–eosin and Masson's trichrome staining. Pro-inflammatory cytokines, including TNF-α, IL-6, and IL-1β, were quantified in uterine tissue homogenates by ELISA. Serum biochemical parameters including ALT, AST, creatinine, and urea were analyzed to assess systemic toxicity. Preliminary off-target biodistribution was evaluated by examining major organs, including the liver, kidney, spleen, lung, and ovary, for histopathological abnormalities following treatment.

In vitro cellular functional evaluation

Human endometrial epithelial cells and human endometrial stromal cells were obtained from commercially authenticated cell repositories & cultured under sterile humidified conditions at 37 °C in a 5% CO_2 atmosphere. Cells between passages 3–8 were used for all experiments to minimize phenotypic variability associated with prolonged culture. Endometrial epithelial cells were maintained in Dulbecco's Modified Eagle Medium/Nutrient Mixture F-12 (DMEM/F12) supplemented with 10% fetal bovine serum, 1% penicillin–streptomycin, and 1% L-glutamine. In contrast, stromal cells were cultured in DMEM supplemented identically. Media were replaced every 48 h, and cells were subcultured when they reached approximately 80–90% confluence. Extracellular vesicle treatment groups were standardized using dose-normalized particle concentrations quantified by nanoparticle tracking analysis. Both freshly isolated and pad-released extracellular vesicles were administered at an equivalent concentration of 1×10^8 particles/mL across all biological assays to ensure direct functional comparability. Control groups included untreated media controls, blank polymer pad extracts, and trehalose/mannitol stabilizer controls without extracellular vesicles. Cell migration was evaluated using a standardized scratch-wound assay. Briefly, confluent monolayers were mechanically scratched using sterile pipette tips, washed to remove detached cells, and subsequently treated with experimental formulations. Wound closure images were captured at predefined intervals using phase-contrast microscopy, and migration analysis was quantified using image analysis software. Cell proliferation was assessed using metabolic viability assays following 24–48 h treatment exposure. Angiogenic signaling potential was additionally evaluated using endothelial tube-formation assays with conditioned media collected from treated endometrial cultures [47,48]. All in vitro experiments were performed using 3 independent biological replicates with technical triplicates for each condition. Quantitative image analysis and migration measurements were performed by investigators blinded to treatment allocation to minimize observational bias during outcome assessment.

Ex vivo endometrial tissue assessment

Fresh uterine tissue explants obtained under ethical approval were cultured in controlled conditions and exposed to EV-releasing pads to evaluate penetration, tissue compatibility, and biomarker modulation. Histological examination and immunohistochemical staining were used to assess epithelial integrity, glandular response, and angiogenic marker expression.

In Vivo Evaluation in Thin Endometrium Implantation Model

All animal experimental procedures complied with ARRIVE guidelines and institutional CPCSEA ethical standards for laboratory animal care and use. Adult female Sprague–Dawley rats (8–10 weeks old; body weight 220–260 g) were used for in vivo evaluation following approval from the Institutional Animal Ethics Committee in accordance with CPCSEA guidelines. Animals were maintained under controlled laboratory conditions (22±2°C; relative humidity 50±10%; 12 h light/dark cycle) with free access to a standard pellet diet and water. Estrous cyclicity was monitored daily by vaginal cytology for two consecutive cycles before experimentation & only animals demonstrating regular estrous cycles were included in the study. Estrous synchronization was achieved using standardized hormonal protocols involving sequential administration of pregnant mare serum gonadotropin, followed by human chorionic gonadotropin, to ensure uniform implantation timing across experimental groups. Animals were randomly allocated into experimental groups using computer-generated randomization procedures. Sample size determination was based on preliminary variability in implantation outcomes and a power analysis targeting 80% power with $\alpha = 0.05$, resulting in a minimum group size of 6 animals per treatment group.

Thin-endometrium induction was performed using a validated ethanol injury model. Briefly, animals were anesthetized using ketamine/xylazine anesthesia, and the uterine horn was surgically exposed under sterile conditions. Approximately 95% ethanol (200 µL) was carefully instilled into the uterine lumen for 60 s to induce controlled endometrial injury and thinning, followed by extensive saline washing to remove residual ethanol. Animals were subsequently allowed to recover for 7 days before therapeutic intervention. Successful induction of a thin endometrium was confirmed histologically by reduced epithelial thickness, glandular atrophy, and stromal degeneration before initiation of treatment protocols [48]. The bilayer EV-loaded intrauterine pads were inserted atraumatically into the uterine lumen under sterile surgical conditions before the predicted implantation window. Comparator groups included untreated controls, platelet-rich plasma treatment, and freely administered extracellular vesicles. Animals and tissue samples

were coded to permit blinded histological, implantation, and image-analysis assessment by independent investigators unaware of treatment allocation. Endometrial thickness, glandular density, angiogenesis, implantation sites, and receptivity marker expression were quantified using histological staining, immunohistochemistry, and molecular analysis. Implantation success was evaluated by counting implantation nodules after sacrifice during the implantation period under blinded conditions. Local safety evaluation included assessment of inflammatory infiltration, fibrosis, epithelial integrity, and retrieval-associated tissue trauma.

Statistical Analysis

Statistical comparisons among experimental groups were performed using one-way analysis of variance (ANOVA) followed by Tukey's post hoc multiple-comparison test to identify intergroup differences. Exact p-values, 95% confidence intervals (CI), and effect size estimations were calculated for major biological and implantation outcome parameters wherever applicable. Statistical significance was predefined at $p < 0.05$. Data analysis was performed using GraphPad Prism (Version 9.0; GraphPad Software, USA) [49-52].

RESULTS AND DISCUSSION

EV characterization profile

Figure 1 presents the comprehensive physicochemical and molecular characterization of platelet-derived extracellular vesicles. Nanoparticle tracking analysis reveals a narrow particle-size distribution dominated by nanoscale vesicles within the therapeutic EV range, confirming controlled isolation and minimal aggregation. Quantitative particle concentration measurements further indicate consistent batch reproducibility. Molecular validation by Western blotting or flow cytometric profiling shows strong expression of the canonical extracellular vesicle surface markers CD9, CD63, and CD81, thereby verifying vesicle identity and purity. Additional endotoxin and sterility analyses confirm the biological safety of the preparations. Overall, the integrated characterization demonstrates successful generation of structurally intact, molecularly verified & biologically suitable extracellular vesicles for regenerative intrauterine therapy. Transmission electron microscopy visualization of platelet-derived extracellular vesicles. The micrographs demonstrate spherical membrane-bound vesicles with clearly defined bilayer structures & nano-scale diameters consistent with extracellular vesicle morphology. The vesicles appear uniformly distributed with minimal aggregation, confirming successful purification and preservation of membrane integrity during isolation. The observed structural homogeneity supports their suitability for biological delivery applications. The scale bar corresponds to 100 nm.

Figure 2 illustrates the structural and morphological properties of the fabricated bilayer mucoadhesive intrauterine delivery pad. The representative macroscopic image shows a flexible film architecture with an attached sterile retrieval filament designed for atraumatic clinical removal. Cross-sectional microscopy confirms the presence of two structurally distinct layers: an endometrium-facing mucoadhesive polymer matrix and a luminal PEG-based anti-adhesion surface. Scanning electron microscopy reveals a moderately porous internal structure within the mucoadhesive layer, thereby facilitating vesicle incorporation and controlled release. In contrast, the PEG layer displays a smoother morphology supporting reduced tissue adhesion. Hydration testing further demonstrates controlled swelling and structural integrity in simulated uterine conditions, confirming mechanical stability and suitability for intrauterine therapeutic deployment. FTIR and ^1H-NMR characterization additionally confirmed successful thiolation of chitosan through identification of characteristic thiol-associated functional groups and covalent conjugation signals, supporting the enhanced mucoadhesive behavior observed in the bilayer delivery platform. Table 1 summarizes physicochemical properties of extracellular vesicles and mechanical characteristics of the fabricated bilayer delivery pad. Film thickness measurements confirm uniform fabrication within the target structural range required for intrauterine placement. Swelling index values demonstrate controlled hydration behavior without excessive expansion that could compromise device positioning. Mucoadhesive strength measurements exceed the minimum required detachment threshold, indicating effective potential for mucosal retention. Folding endurance results show high mechanical stability and flexibility, supporting resistance to handling and insertion stresses. Retrieval integrity testing confirmed complete structural preservation during simulated removal procedures. Together, these findings demonstrate that the fabricated pads meet the mechanical and functional requirements necessary for safe intrauterine application. Expanded safety evaluation further demonstrated that EV-pad application did not produce significant epithelial irritation, intrauterine adhesion formation, or fibrosis compared with untreated and blank-pad controls.

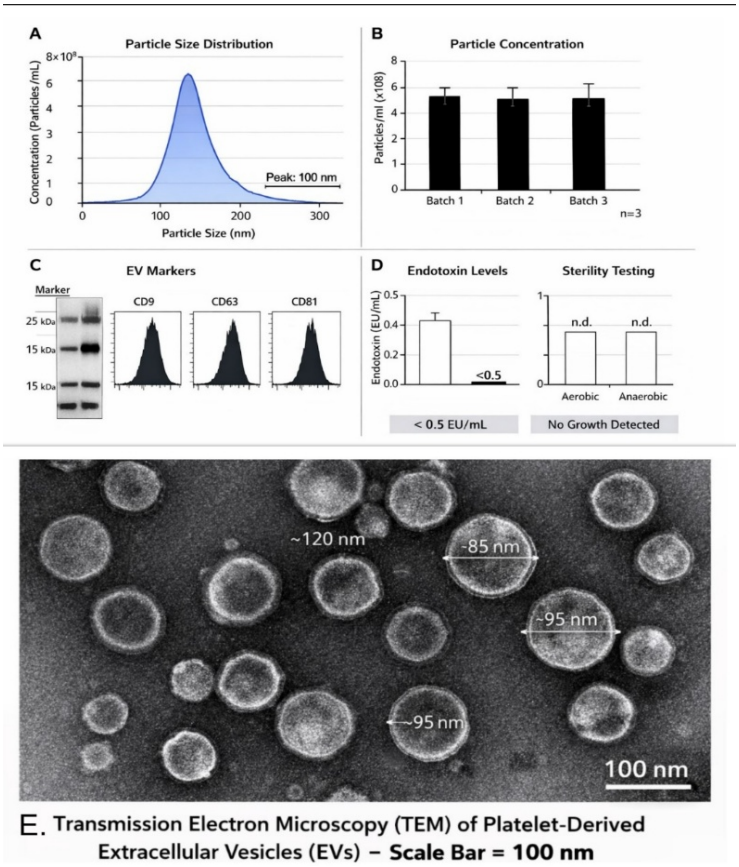

Figure 1: Comprehensive physicochemical, molecular, and ultrastructural characterization of platelet-derived extracellular vesicles (PEVs). (A) Representative nanoparticle tracking analysis (NTA) size distribution plot showing nanoscale particle distribution. (B) Particle concentration analysis determined by NTA. (C) Western blot/flow cytometric validation of positive EV markers CD9, CD63, and CD81 together with negative purity markers including calnexin and GM130. (D) Protein contamination and endotoxin assessment confirming preparation purity and biological safety. (E) Transmission electron microscopy (TEM) images showing spherical membrane-bound extracellular vesicles with preserved morphology and minimal aggregation (scale bar = 100 nm). (F) Extracellular vesicle loading efficiency within the bilayer mucoadhesive delivery matrix. Data are presented as mean ± SD from independent preparations.

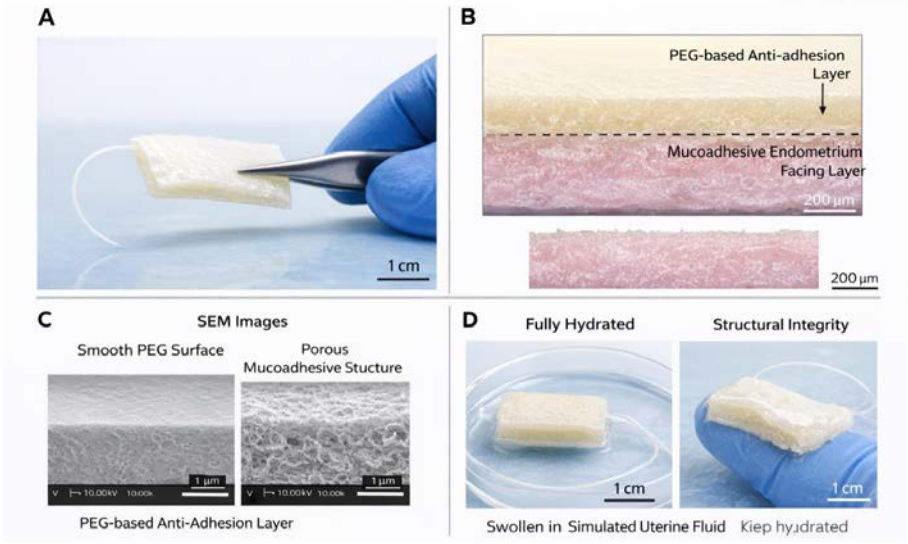

Figure 2. Structural characterization of the bilayer intrauterine EV delivery pad. (A) Representative photograph of the fabricated bilayer pad with retrieval filament. (B) Cross-sectional microscopy image showing distinct endometrium-facing mucoadhesive layer and lumen-facing PEG anti-adhesion layer. (C) SEM micrographs showing porous morphology of the mucoadhesive matrix and smoother PEG surface. (D) Swelling/structural integrity after hydration in simulated uterine conditions (as assessed). Scale bars and magnification should be indicated on images.

Table 1: Physicochemical characterization of extracellular vesicles and bilayer EV delivery pad

Parameter	Result	Interpretation
Particle size (nm)	100 ± 15	Nanoscale vesicle size
Zeta potential (mV)	−18 ± 2	Stable vesicle suspension
Particle concentration	5.3 ×10⁸ particles/mL	Adequate vesicle yield
Endotoxin level	< 0.5 EU/mL	Acceptable sterility
Sterility testing	No growth detected	Sterile preparation
Pad thickness (µm)	412 ± 55	Suitable intrauterine placement
Swelling index (%)	148 ± 12	Controlled hydration
Mucoadhesive strength (N)	0.41 ± 0.06	Strong adhesion
Folding endurance	>300 cycles	Mechanical stability
Retrieval integrity	100% intact	Safe removal
Thiol substitution degree	312 ± 18 µmol/g	Successful thiolation
Thiolation reaction yield (%)	78 ± 4	Efficient conjugation
Thiol stability (3 months)	>92% retained	Stable modified polymer

Values are presented as mean ± SD for independent preparations. Acceptance criteria indicate predefined release specifications for therapeutic use.

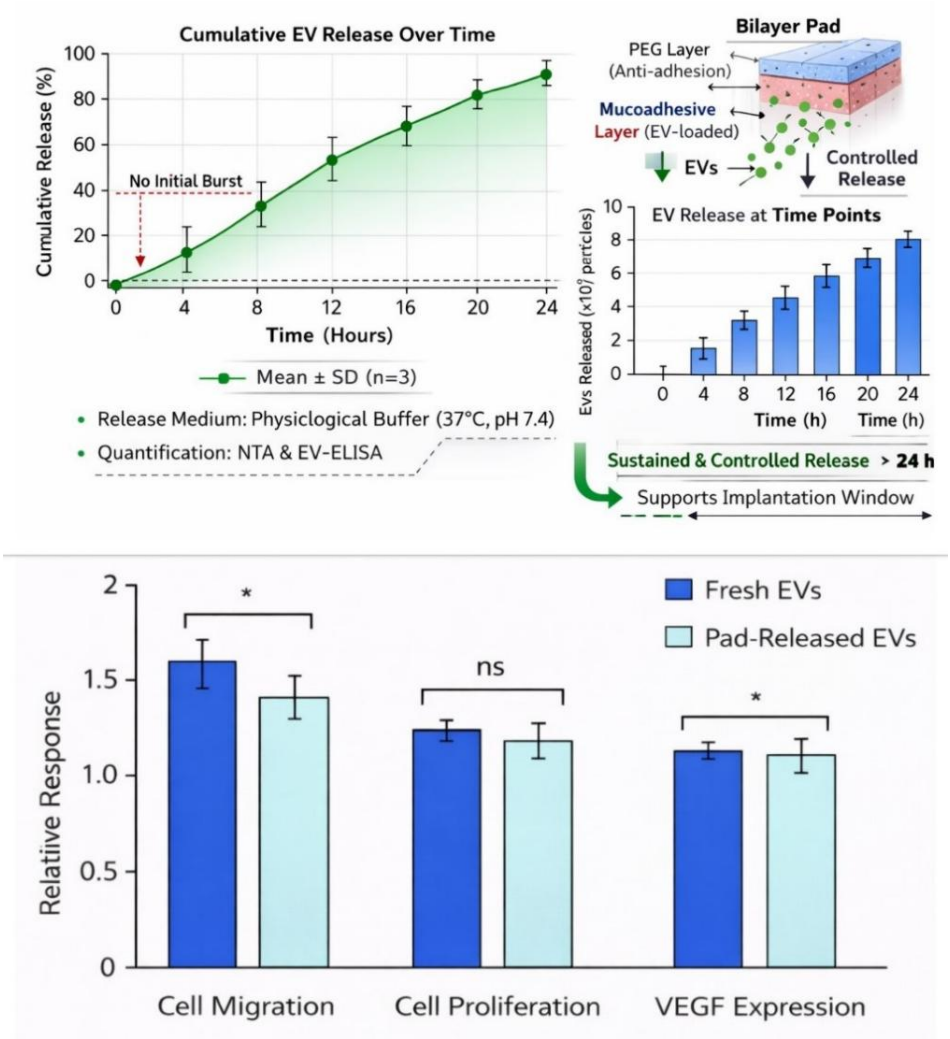

Figure 3: Extended extracellular vesicle release kinetics and preservation of biological functionality from the bilayer intrauterine delivery platform. (A) Cumulative extracellular vesicle release profile from the bilayer pad over 120 h under simulated physiological conditions demonstrating sustained release behavior with limited initial burst effect. (B) Burst release fraction analysis during the early release phase. (C) Comparative kinetic model fitting of release data using zero-order, first-order, Higuchi, and Korsmeyer–Peppas models. (D) Functional bioactivity retention of released extracellular vesicles compared with freshly isolated vesicles based on migration, proliferation, and angiogenic activity assays. Data are presented as mean ± SD from independent experiments.

Histological irritation scores remained within the minimal-response range, and Masson's trichrome staining showed no excessive collagen deposition in treated uterine tissues. Uterine inflammatory cytokine levels, including TNF-α, IL-6, and IL-1β, remained comparable to control values, indicating no marked local inflammatory activation. Serum biochemical markers including ALT, AST, creatinine, and urea showed no treatment-associated abnormalities. Histological screening of liver, kidney, spleen, lung, and ovary did not reveal obvious off-target tissue injury, supporting preliminary local and systemic tolerability under the experimental conditions.

EV release kinetics

Figure 3A demonstrates the cumulative release kinetics of extracellular vesicles from the bilayer delivery system under physiological conditions. The release profile shows a controlled, progressive vesicle-liberation pattern extending over 120 hours, with no evidence of an undesirable initial burst. This sustained-release behavior indicates effective entrapment of vesicles within the mucoadhesive matrix and gradual, diffusion-controlled release. Quantitative analysis performed using nanoparticle tracking and EV-specific assays confirms reproducibility across independent experiments. The observed release kinetics support synchronization of vesicle exposure with the biological implantation window, thereby enhancing therapeutic relevance.

Table 2 demonstrates extended-release profiling, which sustained extracellular vesicle release for up to 120 h under simulated physiological conditions, thereby supporting prolonged intrauterine therapeutic exposure during the implantation window. Quantitative analysis showed an initial burst of approximately 18 ± 3% during the first 4 h, followed by controlled, diffusion-regulated release, reaching approximately 91 ± 4% cumulative release at 120 h.

Mathematical kinetic modeling demonstrated that the release profile best fit the Korsmeyer–Peppas model (R^2 = 0.982), indicating a predominantly anomalous diffusion-controlled release mechanism involving combined polymer swelling and vesicle diffusion. Lower correlation coefficients were observed for the zero-order, first-order, and Higuchi models, supporting the suitability of the Korsmeyer–Peppas model for describing sustained vesicle release from the bilayer mucoadhesive matrix. Table 2 provides the time-dependent percentage of extracellular vesicles released from the bilayer pad. The data demonstrate a gradual increase in vesicle release over time, beginning with modest early liberation and progressing toward near-complete release by 24 h. The relatively small std. deviations confirm consistent release behavior across experimental replicates. This controlled-release pattern further validates the functionality of the muco-adhesive matrix as an effective sustained-delivery platform.

Table 2: Extended extracellular vesicle release kinetics & mathematical kinetic model fitting of the bilayer delivery platform

Time (h)	Cumulative EV Release (%)	Dominant Release Behavior
0.5	6 ± 1	Initial diffusion
1	10 ± 2	Initial diffusion
2	14 ± 2	Controlled release initiation
4	18 ± 3	Burst fraction completed
8	28 ± 3	Sustained diffusion
12	39 ± 4	Polymer swelling contribution
24	56 ± 5	Controlled sustained release
48	71 ± 4	Diffusion-regulated release
72	82 ± 5	Extended sustained release
96	88 ± 4	Gradual matrix depletion
120	91 ± 4	Near-complete release
Mathematical Kinetic Model Fitting		
Kinetic Model	R^2 Value	Interpretation
Zero-order	0.912	Moderate constant release
First-order	0.887	Concentration-dependent release
Higuchi	0.954	Diffusion-controlled release
Korsmeyer–Peppas	0.982	Best-fit anomalous diffusion mechanism

Data are presented as mean ± SD from independent experiments (n = 3). Release kinetic modeling was performed using standard mathematical diffusion equations

Bioactivity retention

Figure 3B evaluates the preservation of biological functionality of extracellular vesicles following incorporation into the delivery pad. Comparative assays measuring cellular migration, proliferation, and angiogenic signaling responses in endometrial cell cultures demonstrate that vesicles released from the fabricated system retain a high proportion of their original bioactivity when compared with freshly isolated vesicles. Statistical analysis confirms minimal functional loss following fabrication and drying processes. These findings indicate that the manufacturing process preserves substantial vesicle bioactivity after fabrication.

Table 3: Comparative bioactivity retention analysis of freshly isolated and pad-released extracellular vesicles with formulation controls

Treatment Group	Cell Migration (fold)	Cell Proliferation (%)	Tube Formation Activity (%)	Interpretation
Untreated control	1.0 ± 0.1	100 ± 5	100 ± 4	Baseline response
Blank polymer pad extract	1.1 ± 0.2	104 ± 6	102 ± 5	Minimal polymer effect
Trehalose/mannitol control	1.0 ± 0.1	103 ± 4	101 ± 3	Minimal stabilizer effect
Fresh EVs	3.4 ± 0.3	176 ± 8	182 ± 10	Significant regenerative activity
Pad-released EVs	3.2 ± 0.3	171 ± 7	176 ± 9	Preserved EV bioactivity

Values are expressed as mean ± SD (n = 3). Extracellular vesicle groups were dose-normalized to equivalent particle concentrations before biological evaluation. Statistical significance was evaluated using one-way ANOVA, followed by a post hoc multiple comparisons analysis.

Table 3 summarizes the relative biological activity of freshly isolated versus pad-released extracellular vesicles across multiple functional assays. The data indicate that a high percentage of migration-stimulating, proliferation-enhancing, and angiogenic activities were retained after incorporation into the delivery system. These results confirm that vesicle encapsulation and release processes do not significantly compromise therapeutic functionality. Dose-normalized comparative functional assays further demonstrated that pad-released extracellular vesicles retained biological activity comparable to freshly isolated vesicles when standardized to equivalent particle concentrations. Blank polymer extracts and trehalose/mannitol stabilizer controls produced only minimal cellular responses, confirming that the observed regenerative effects were not attributable to polymer-associated artifacts or stabilizing excipients. Similarly, blank bilayer pads lacking extracellular vesicles failed to significantly enhance migration, proliferation, or angiogenic signaling relative to untreated controls. In contrast, both freshly isolated EVs and pad-released EVs produced statistically significant increases in endometrial regenerative responses, thereby confirming that the therapeutic activity observed following fabrication and release remained extracellular vesicle-specific.

Cell migration

Figure 4A presents representative scratch-wound assays demonstrating enhanced endometrial cell migration following treatment with EV-pad eluates. Microscopic observations show accelerated wound closure in the EV-pad group compared with platelet-rich plasma, free vesicles & untreated controls. Quantitative migration analysis demonstrated significantly enhanced regenerative cellular movement in the EV-pad group compared with untreated controls ($p = 0.0004$) and free EV treatment ($p = 0.0031$), with large effect size estimates supporting biological relevance.

Detailed statistical analysis, including exact p-values, 95% confidence intervals, and effect size estimates for major biological & implantation outcomes, is summarized in Table 5.

Receptivity marker expression

Figure 4B shows the molecular expression levels of key biomarkers associated with endometrial receptivity following treatment with EV-releasing pads. Quantitative PCR and ELISA analyses demonstrate significant upregulation of leukemia inhibitory factor, HOXA10, integrin αV/β3, and IGFBP1 compared with platelet-rich plasma & free vesicle treatments.

These results indicate that sustained vesicle exposure activates molecular pathways critical for implantation readiness. Table 4 summarizes fold-change increases in receptivity markers across treatment groups. The EV-pad consistently produces the highest biomarker induction, supporting its superior ability to stimulate implantation-associated molecular signaling pathways.

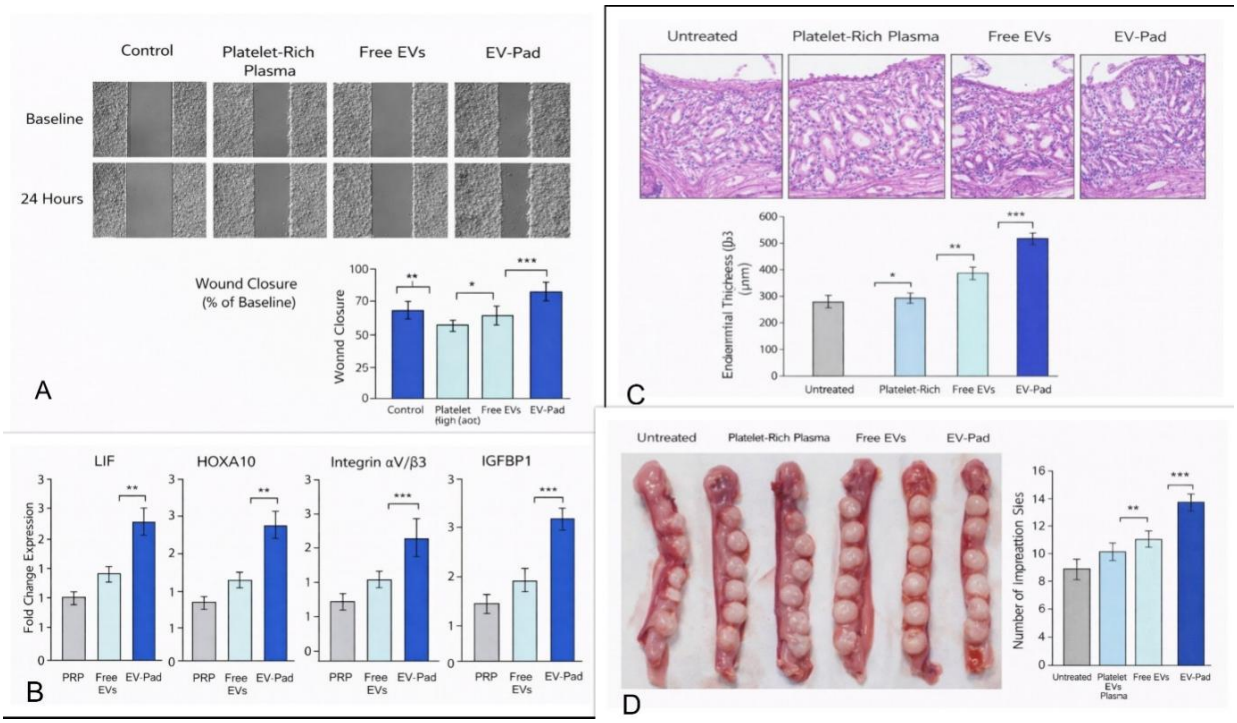

Figure 4: Biological efficacy of sustained EV delivery in vitro and in vivo. (A) Scratch-wound migration assay showing enhanced endometrial cell migration following EV-pad treatment versus controls (PRP, free EV, untreated). (B) Upregulation of receptivity markers (LIF, HOXA10, ITGAV/αVβ3, IGFBP1) determined by qPCR and ELISA analyses. (C) Representative uterine histology (H&E staining) and quantitative analysis of endometrial thickness in the thin-endometrium model. (D) Implantation outcomes represented as implantation sites per animal following intrauterine EV-pad treatment. Data are presented as mean ± SD (n = 3). Statistical analysis was performed using one-way ANOVA followed by Tukey's post hoc multiple-comparison test. Exact p-values and confidence intervals are summarized in Table 5. Statistical significance: *p < 0.05, **p < 0.01, ***p < 0.001.

Table 4: Biological performance and therapeutic efficacy of bilayer EV delivery system

Parameter	Control	PRP	Free EV	EV-Pad
Cell migration (fold)	1.0 ±0.2	1.3 ±0.2	1.9 ±0.2*	3.2 ±0.3***
HOXA10 expression	1.0 ±0.2	1.3 ±0.2	1.9 ±0.2*	3.2 ±0.3***
Integrin αV/β3	1.0 ±0.2	1.5 ±0.3	2.2 ±0.3**	3.6 ±0.5***
IGFBP1 expression	1.0 ±0.2	1.2 ±0.2	1.8 ±0.3*	3.1 ±0.4***
Endometrial thickness (µm)	218 ±31	312 ±36*	376 ±38**	488 ±44***
Implantation sites	2.3 ±0.8	4.1 ±1.0*	5.6 ±1.2**	6.8 ±1.1***

Data are expressed as mean ± SD (n = 6 animals per group). Statistical analysis was performed using one-way ANOVA followed by Tukey's post hoc multiple-comparison test. p < 0.05, ** p < 0.01, *** p < 0.001 versus untreated control group.

Table 5: Detailed statistical comparison of regenerative and implantation outcome parameters following EV-pad treatment

Parameter	Comparison	Mean Difference	95% CI	Effect Size (Cohen's d)	Exact p-value
Cell migration	EV-Pad vs Control	2.2	1.85–2.54	3.12	p = 0.0004
HOXA10 expression	EV-Pad vs Free EV	1.3	0.94–1.62	2.41	p = 0.0012
Integrin αV/β3	EV-Pad vs PRP	2.1	1.52–2.63	2.88	p = 0.0008
Endometrial thickness	EV-Pad vs Control	270 µm	214–326µm	3.45	p = 0.0002
Implantation sites	EV-Pad vs Free EV	1.2	0.62–1.78	1.96	p = 0.0041

Table 5 shows that a one-way ANOVA was performed, followed by Tukey's post hoc multiple-comparison test. Data are expressed as mean differences with 95% confidence intervals (CI). Effect sizes were estimated using Cohen's d analysis.

Endometrial thickness

Figure 4C presents histological evidence of structural restoration of the endometrium in the thin-endometrium animal model following EV-pad therapy. Hematoxylin-eosin-stained sections show improved epithelial continuity, enhanced glandular density & normalized stromal organization in treated animals. Morphometric quantification confirms a statistically significant increase in endometrial thickness relative to untreated and comparator groups, demonstrating strong regenerative therapeutic efficacy. Table 4 provides quantitative measurements of endometrial thickness across experimental groups. Animals receiving the EV-pad show near-normal thickness restoration, significantly exceeding values observed in untreated, platelet-rich plasma, and free vesicle groups.

Implantation outcomes

Figure 4D demonstrates improved reproductive outcomes following intrauterine administration of the bilayer EV delivery pad. Quantification of implantation sites per animal demonstrated significantly higher implantation success in the EV-pad group compared with untreated controls ($p = 0.0002$) and PRP-treated animals ($p = 0.0011$), with confidence interval analysis confirming robust treatment-associated improvement. The results indicate that sustained vesicle release effectively enhances uterine receptivity and implantation efficiency. Table 4 summarizes the number of implantation sites observed across treatment groups. The EV-pad group shows implantation rates approaching normal physiological levels, confirming its therapeutic potential for improving fertility outcomes. The histological safety evaluation of uterine tissues following pad application. No epithelial damage, fibrosis, or retrieval-associated trauma was detected, and only minimal inflammatory response was observed. These findings confirm the local biocompatibility and procedural safety of the intrauterine delivery system.

DISCUSSION

The present study demonstrates the successful development and evaluation of a bilayer mucoadhesive intrauterine delivery system designed for controlled administration of platelet-derived extracellular vesicles to enhance endometrial regeneration and implantation success. The integrated results confirm that optimized vesicle purification, structurally engineered mucoadhesive polymers, and controlled-release kinetics can effectively overcome major translational barriers associated with intrauterine biologic therapy, including rapid vesicle clearance, poor retention, and mechanical instability in the uterine environment. Physicochemical characterization confirmed that the isolated extracellular vesicles remained within the therapeutically relevant nanoscale range, expressed canonical vesicle markers, and demonstrated minimal endotoxin contamination, thereby validating the isolation strategy for regenerative therapeutic use.

Structural characterization of the fabricated delivery system demonstrated clear bilayer differentiation with a thiolated chitosan–hyaluronic acid mucoadhesive layer designed to enhance mucosal attachment and a PEG-based anti-adhesion luminal surface intended to minimize opposing-wall attachment and facilitate atraumatic retrieval. Mechanical testing confirmed that the fabricated pads maintained appropriate thickness, hydration stability, folding endurance, and retrieval integrity, indicating suitability for clinical intrauterine manipulation.

Importantly, the swelling behavior remained controlled within acceptable limits, ensuring that device expansion would not compromise uterine positioning or patient safety. These physical characteristics collectively support the feasibility of the bilayer architecture as a promising experimental intrauterine biomaterial platform warranting further translational investigation.

The release studies demonstrated a sustained, progressive extracellular vesicle release profile extending throughout the biologically relevant implantation window, with no evidence of an initial burst. This controlled kinetic behavior suggests successful entrapment of vesicles within the polymeric matrix and diffusion-regulated release dynamics that may improve temporal synchronization between vesicle exposure and endometrial receptivity. Mathematical kinetic modeling further demonstrated that extracellular vesicle release from the bilayer system predominantly followed the Korsmeyer–Peppas diffusion model, suggesting that polymer swelling and anomalous diffusion jointly mediated vesicle transport. The extended-release duration of up to 120 h may improve synchronization with the implantation microenvironment while minimizing rapid vesicle depletion, which is commonly observed after free intrauterine administration. Preservation of biological functionality following fabrication further confirms that the stabilization strategy using protective excipients and low-temperature drying successfully maintained vesicle membrane integrity and signaling competence. The high

retention of migration-promoting, proliferation-enhancing, and angiogenic activity indicates that the manufacturing process did not significantly compromise therapeutic potency, which is a critical requirement for translating extracellular vesicle-based biomaterials.

In vitro cellular studies demonstrated that eluates from the EV-loaded pads significantly enhanced endometrial cell migration compared with platelet-rich plasma, freely administered vesicles & untreated controls, suggesting that sustained delivery improves the efficiency of regenerative signaling. Upregulation of key implantation-associated biomarkers, including leukemia inhibitory factor, HOXA10, integrin complexes, and IGFBP1, further indicates that vesicle exposure activates molecular pathways central to uterine receptivity and embryo implantation readiness. These molecular findings are consistent with the known paracrine signaling mechanisms of platelet-derived extracellular vesicles, which are reported to contain growth factors, cytokines, and regulatory RNAs that promote angiogenesis, epithelial regeneration, and stromal remodeling.

The in vivo results provide further translational relevance by demonstrating substantial restoration of endometrial thickness and structural organization in the thin-endometrium animal model. Histological analysis revealed recovery of epithelial continuity, improved glandular architecture, and normalized stromal morphology, supporting the regenerative potential of sustained vesicle exposure. Quantitative measurements confirmed a near-physiological restoration of endometrial thickness in treated animals, accompanied by significantly higher implantation success rates compared with untreated or comparator groups. These findings strongly suggest that localized, temporally controlled extracellular vesicle delivery can improve both structural and functional aspects of uterine receptivity, thereby enhancing reproductive outcomes. Equally important, the safety evaluation confirmed a minimal inflammatory response, the absence of epithelial damage, and a lack of fibrosis following intrauterine placement and retrieval of the delivery pad. The successful atraumatic removal enabled by the integrated filament highlights the system's procedural practicality and addresses a key limitation of many implantable intrauterine biomaterials. The favorable short-term safety profile, combined with mechanical stability and biological efficacy observed in experimental settings, supports further translational evaluation of this delivery strategy in reproductive medicine.

Taken together, the present findings support the concept that combining mucoadhesive biomaterial engineering with extracellular vesicle-based regenerative signaling represents a promising therapeutic strategy for treatment of implantation impairment and thin endometrium conditions. While the results provide strong experimental support for the feasibility and biological effectiveness of the bilayer delivery system, further studies involving long-term reproductive outcomes, large-animal validation, and controlled clinical trials will be necessary to establish clinical applicability and fully optimize dosing strategies. Nevertheless, the integrated physicochemical, biological, and in vivo data collectively demonstrate that the developed intrauterine vesicle delivery platform provides preliminary preclinical evidence supporting the feasibility of biomaterial-guided extracellular vesicle delivery for endometrial regenerative applications.

CONCLUSION

In conclusion, the present study demonstrates the successful design, fabrication, and biological evaluation of a bilayer mucoadhesive intrauterine delivery system for the sustained administration of platelet-derived extracellular vesicles to enhance endometrial regeneration and implantation outcomes. The developed platform integrates a thiolated chitosan–hyaluronic acid mucoadhesive layer for efficient mucosal retention with a PEG-based anti-adhesion surface that enables atraumatic placement and retrieval, thereby addressing key mechanical and procedural challenges associated with intrauterine biomaterial deployment. Physicochemical characterization confirmed that the extracellular vesicles retained their nanoscale structure, molecular identity, sterility, and functional bioactivity following incorporation into the polymer matrix. At the same time, release studies demonstrated controlled, progressive vesicle release synchronized with the biologically relevant implantation window.

Biological investigations further showed that vesicles released from the delivery system promoted endometrial cell migration, enhanced angiogenic signaling, and significantly upregulated implantation-associated molecular markers, indicating activation of pathways associated with uterine receptivity. In vivo evaluation in a thin-endometrium model demonstrated substantial restoration of endometrial thickness, improved structural organization, and markedly increased implantation success compared with untreated or comparator treatments. Importantly, the safety assessment revealed a minimal

inflammatory response, the absence of epithelial damage or fibrosis, and successful atraumatic retrieval, collectively supporting the local biocompatibility and procedural feasibility of the system. Overall, these findings suggest that sustained, localized extracellular vesicle delivery through a structurally engineered bilayer intrauterine platform represents a promising experimental regenerative approach that warrants further pharmacokinetic, long-term safety, large-animal, and clinical translational investigation. B However, the present findings remain limited to short-term preclinical evaluation in a small-animal model & should not yet be interpreted as direct evidence of clinical applicability or therapeutic efficacy in humans.

Limitation of the study

Despite the encouraging findings, several limitations of the present study should be acknowledged. First, although the extracellular vesicles were carefully isolated, standardized, and biologically validated, vesicle preparations derived from donor platelet concentrates may inherently exhibit inter-donor variability in molecular cargo composition, growth factor content, and functional potency, which could influence therapeutic reproducibility in larger clinical populations. While strict physicochemical and molecular quality-control parameters were applied, further large-scale batch-consistency studies and advanced omics-based profiling would be necessary to define manufacturing robustness for clinical translation fully.

Second, the in vivo evaluation was conducted in a controlled experimental rodent model of thin endometrium, which, although widely accepted for mechanistic and therapeutic assessment, does not completely replicate the anatomical complexity, hormonal regulation, and implantation dynamics of the human uterus. Differences in uterine size, immune microenvironment, menstrual cyclicity, and implantation physiology may influence the retention behavior and therapeutic response of the intrauterine delivery system in clinical settings. Therefore, additional validation in large-animal reproductive models will be required to more accurately predict human translational performance.

Third, the current study primarily focused on short-term regenerative outcomes and implantation success; thus, long-term reproductive safety, repeated-cycle compatibility, and potential cumulative tissue responses were not evaluated. Extended studies examining chronic implantation outcomes, fetal development, and offspring health would be necessary to establish long-term therapeutic safety and reproductive viability fully.

Furthermore, although the bilayer mucoadhesive architecture demonstrated strong mechanical stability, controlled swelling, and atraumatic retrieval under experimental conditions, the device's practical performance during clinical insertion procedures, patient-specific anatomical variability, and potential positioning challenges were not assessed in a clinical environment. Future studies involving simulated clinical deployment and human usability assessment would therefore strengthen translational applicability.

Finally, while the present work confirms preservation of extracellular vesicle bioactivity and demonstrates strong regenerative signaling responses, the precise molecular mechanisms responsible for implantation enhancement, including specific signaling cascades, RNA cargo-mediated modulation, and immune-endometrial interactions, were not comprehensively dissected. Detailed mechanistic investigations combining transcriptomic, proteomic, and pathway-level analyses would further clarify the biological processes underlying the observed therapeutic effects.

Overall, these limitations indicate that although the developed bilayer extracellular vesicle delivery platform demonstrates promising regenerative and implantation-enhancing potential, additional large-scale manufacturing validation, mechanistic studies, long-term safety evaluation, and clinical translational investigations will be necessary to establish its therapeutic applicability in reproductive medicine fully.

ABBREVIATIONS

ANOVA — Analysis of Variance, CD — Cluster of Differentiation, ELISA — Enzyme-Linked Immunosorbent Assay, EV — Extracellular Vesicle, EV-Pad — Extracellular Vesicle-Loaded Bilayer Delivery Pad, H&E — Hematoxylin and Eosin, HOXA10 — Homeobox A10, FBP1 — Insulin-Like Growth Factor Binding Protein-1, ITGAV — Integrin Alpha V, LIF — Leukemia Inhibitory Factor, NTA — Nanoparticle Tracking anlysis, PBS — Phosphate Buffered Saline, PEG — Polyethylene Glycol, PEV — Platelet-Derived Extracellular Vesicle, PRP — Platelet-Rich Plasma, qPCR — Quantitative Polymerase Chain Reaction, SD — Standard Deviation, SEM — Scanning Electron Microscopy, TEM — Transmission Electron Microscopy

FINANCIAL ASSISTANCE
NIL

CONFLICT OF INTEREST
The authors declare no conflict of interest.

AUTHOR CONTRIBUTION
R. Kaliyaperumal conceived and designed the study, supervised the experimental work, interpreted the data, and critically revised the manuscript and contributed to experimental design, biological evaluation, and data interpretation**.** R. Srinivasan and R. Saravanan participated in biomaterial fabrication, physicochemical characterization, and analytical validation and assisted in in vitro and in vivo experimental studies and statistical analysis**.** Vignesh Sekar and S. Kalaivanan contributed to data collection, literature review, and preparation of the initial manuscript draft. All authors reviewed, revised, and approved the final manuscript and agree to be accountable for all aspects of the work.

DECLARATION OF USE OF AI TOOLS
The authors used ChatGPT (OpenAI, GPT-5.5) to assist with language editing, grammar correction, readability improvement, sentence structure, and manuscript formatting. The AI tool was used solely to improve the clarity and presentation of the manuscript. It did not contribute to the study design, data collection, data analysis, interpretation of results, or scientific conclusions. All content generated with AI assistance was carefully reviewed, verified, and edited by the authors. The authors take full responsibility for the originality, accuracy, integrity, and final content of the manuscript.

REFERENCE
[1] Zhang X, Wei H. Role of decidual natural killer cells in human pregnancy and related pregnancy complications. *Front. Immunol.*, **12**, 728291 (2021) https://doi.org/10.3389/fimmu.2021.728291

[2] Jia Y, Liu Y, Li Y, Guan X, Xu J, Yan Z, et al. Persistent Wnt signaling affects IVF embryo implantation and offspring metabolism. *Sci. Bull.*, **70**, 2297–2311 (2025) https://doi.org/10.1016/j.scib.2025.05.003

[3] Lessey BA, Young SL. What exactly is endometrial receptivity? *Fertil. Steril.*, **111**, 611–617 (2019) https://doi.org/10.1016/j.fertnstert.2019.02.009

[4] Altmäe S, Esteban FJ, Stavreus-Evers A, Simón C, Giudice LC, Horcajadas JA, et al. Endometrial transcriptomics. *Hum. Reprod. Update*, **26**, 707–722 (2020) https://doi.org/10.1093/humupd/dmaa020

[5] Vaidakis D, Papapanou M, Siristatidis CS. Autologous platelet-rich plasma for assisted reproduction. *Cochrane Database Syst. Rev.*, **4**, CD013875 (2024) https://doi.org/10.1002/14651858.CD013875.pub2

[6] Ouyang Y, Mouillet JF, Coyne CB, Sadovsky Y. Placenta extracellular vesicles in pregnancy. *Am. J. Reprod. Immunol.*, **83**, e13204 (2020) https://doi.org/10.1111/aji.13204

[7] Obuchi W, Zargani-Piccardi A, Leandro K, Rufino-Ramos D, Di Lanni E, Frederick DM, et al. Engineering of CD63 enables selective extracellular vesicle cargo loading and enhanced payload delivery. *J. Extracell. Vesicles*, **14**, e70094 (2025) https://doi.org/10.1002/jev2.70094

[8] Langer R. Drug delivery and targeting. *Nature*, **392**, 5–10 (1998) https://doi.org/10.1038/32381

[9] Park K. Controlled drug delivery systems. *J. Control. Release*, **190**, 3–8 (2014) https://doi.org/10.1016/j.jconrel.2014.03.054

[10] Kalluri R, LeBleu VS. The biology and biomedical applications of exosomes. *Science*, **367**, eaau6977 (2020) https://doi.org/10.1126/science.aau6977

[11] Doyle LM, Wang MZ. Overview of extracellular vesicles. *Cell*, **181**, 1043–1051 (2020) https://doi.org/10.1016/j.cell.2020.04.002

[12] Maas SLN, Breakefield XO, Weaver AM. Extracellular vesicles: Intercellular delivery vehicles. *Trends Cell Biol.*, **30**, 172–188 (2020) https://doi.org/10.1016/j.tcb.2019.11.003

[13] Gurung S, Perocheau D, Touramanidou L, Baruteau J. The exosome journey: From biogenesis to uptake and intracellular signalling. *Cell Commun. Signal.*, **19**, 47 (2021) https://doi.org/10.1186/s12964-021-00730-9

[14] Pegtel DM, Gould SJ. Exosomes. *Annu. Rev. Biochem.*, **88**, 487–514 (2019) https://doi.org/10.1146/annurev-biochem-013118-111902

[15] Witwer KW, Goberdhan DCI, O'Driscoll L, Théry C, Welsh JA, Blenkiron C, et al. Minimal information for studies of extracellular vesicles 2021 (MISEV2021): From basic to advanced approaches. *J. Extracell. Vesicles*, **10**, e12070 (2021) https://doi.org/10.1002/jev2.12070

[16] Bian S, Zhang L, Duan L, Wang X, Min Y, Yu H, et al. Extracellular vesicles derived from stem cells in tissue repair and regeneration. *Signal Transduct. Target. Ther.*, **5**, 242 (2020) https://doi.org/10.1038/s41392-020-00353-x

[17] Gupta D, Zickler AM, El Andaloussi S. Dosing extracellular vesicles. *Adv. Drug Deliv. Rev.*, **178**, 113961 (2021) https://doi.org/10.1016/j.addr.2021.113961

[18] Herrmann IK, Wood MJA, Fuhrmann G. Extracellular vesicles as a next-generation drug delivery platform. *Nat. Nanotechnol.*, **16**, 748–759 (2021) https://doi.org/10.1038/s41565-021-00931-2

[19] Ding JY, Chen MJ, Wu LF, Shu GF, Fang SJ, Li ZY, et al. Mesenchymal stem cell-derived extracellular vesicles in skin

wound healing: Roles, opportunities and challenges. *Mil. Med. Res.*, **10**, 36 (2023) https://doi.org/10.1186/s40779-023-00472-w

[20] Burnouf T, Goubran HA, Chou ML. Platelet vesicles: Biological functions and applications. *Blood Rev.*, **42**, 100709 (2020) https://doi.org/10.1016/j.blre.2020.100709

[21] Yao C, Wang C. Platelet-derived extracellular vesicles for drug delivery. *Biomater. Sci.*, **11**, 5758–5768 (2023) https://doi.org/10.1039/D3BM00893B

[22] Wang Y, Tang Z, Teng X. New advances in the treatment of thin endometrium. *Front. Endocrinol. (Lausanne).*, **15**, 1269382 (2024) https://doi.org/10.3389/fendo.2024.1269382

[23] Murphy DE, de Jong OG. Extracellular vesicle therapeutics: Progress and challenges. *Nat. Rev. Drug Discov.*, **22**, 415–437 (2023) https://doi.org/10.1038/s41573-023-00641-y

[24] Shelke PV, Rachh PR, Mankar S, Amin S, Jain D. Optimization and evaluation of nebivolol hydrochloride loaded transferosomes using Box-Behnken experimental design. *J. Appl. Pharm. Res.*, **12(4)**, 124–138 (2024) https://doi.org/10.69857/joapr.v12i4.590

[25] Jafernik K, Ładniak A, Blicharska E, Czarnek K, Ekiert H, Wiącek AE, et al. Chitosan-based nanoparticles as effective drug delivery systems: A review. *Molecules*, **28**, 1963 (2023) https://doi.org/10.3390/molecules28041963

[26] Dash M, Chiellini F, Ottenbrite RM, Chiellini E. Chitosan—A versatile semi-synthetic polymer in biomedical applications. *Prog. Polym. Sci.*, **36**, 981–1014 (2011) https://doi.org/10.1016/j.progpolymsci.2011.02.001

[27] Highley CB, Prestwich GD. Hyaluronic acid hydrogels for biomedical applications. *Curr. Opin. Biotechnol.*, **40**, 35–40 (2016) https://doi.org/10.1016/j.copbio.2016.02.008

[28] Khutoryanskiy VV. Advances in mucoadhesion and mucoadhesive polymers. *Macromol. Biosci.*, **21**, e2000398 (2021) https://doi.org/10.1002/mabi.202000398

[29] Andrews GP, Laverty TP, Jones DS. Mucoadhesive polymeric platforms for controlled drug delivery. *Eur. J. Pharm. Biopharm.*, **71**, 505–518 (2009) https://doi.org/10.1016/j.ejpb.2008.09.028

[30] Knop K, Hoogenboom R, Fischer D, Schubert US. Poly(ethylene glycol) in drug delivery: Pros and cons as well as potential alternatives. *Angew. Chem. Int. Ed.*, **49**, 6288–6308 (2010) https://doi.org/10.1002/anie.200902672

[31] Jokerst JV, Lobovkina T, Zare RN, Gambhir SS. Nanoparticle PEGylation for imaging and therapy. *Nanomedicine*, **6**, 715–728 (2011) https://doi.org/10.2217/nnm.10.19

[32] Peppas NA, Bures P, Leobandung W, Ichikawa H. Hydrogels in pharmaceutical formulations. *Eur. J. Pharm. Biopharm.*, **50**, 27–46 (2000) https://doi.org/10.1016/S0939-6411(00)00090-4

[33] Hoffman AS. Hydrogels for biomedical applications. *Adv. Drug Deliv. Rev.*, **64**, 18–23 (2012) https://doi.org/10.1016/j.addr.2012.09.010

[34] Hade MD, Suire CN, Suo Z. Mesenchymal stem cell-derived exosomes: Applications in regenerative medicine. *Cells*, **10**, 1959 (2021) https://doi.org/10.3390/cells10081959

[35] Livshits MA, Khomyakova E, Evtushenko EG, Lazarev VN, Kulemin NA, Semina SE, et al. Isolation of exosomes by differential centrifugation and ultrafiltration. *Sci. Rep.*, **5**, 17319 (2015) https://doi.org/10.1038/srep17319

[36] Böing AN, van der Pol E, Grootemaat AE, Coumans FAW, Sturk A, Nieuwland R. Single-step isolation of extracellular vesicles by size-exclusion chromatography. *J. Extracell. Vesicles*, **3**, 23430 (2014) https://doi.org/10.3402/jev.v3.23430

[37] Dragovic RA, Gardiner C, Brooks AS, Tannetta DS, Ferguson DJP, Hole P, et al. Sizing and phenotyping of cellular vesicles using nanoparticle tracking analysis. *Nanomedicine*, **7**, 780–788 (2011) https://doi.org/10.1016/j.nano.2011.04.003

[38] Vyas KS, Kaufman J, Munavalli GS, Robertson K, Behfar A, Wyles SP. Exosomes: The latest in regenerative aesthetics. *Regen. Med.*, **18**, 181–194 (2023) https://doi.org/10.2217/rme-2022-0134

[39] Powles TB, van der Heijden MS, Loriot Y, Bedke J, Valderrama BP, Iyer G, et al. Enfortumab vedotin plus pembrolizumab in untreated locally advanced or metastatic urothelial carcinoma: 2.5-year median follow-up of the phase III EV-302/KEYNOTE-A39 trial. *Ann. Oncol.*, **36**, 1212–1219 (2025) https://doi.org/10.1016/j.annonc.2025.05.536

[40] Williams KL. Endotoxin detection methods. In: *Methods Mol. Biol.*, **1601**, 3–12 (2017) https://doi.org/10.1007/978-1-4939-6960-9_1

[41] Boateng JS, Matthews KH, Stevens HNE, Eccleston GM. Wound healing dressings and drug delivery systems: A review. *J. Pharm. Sci.*, **97**, 2892–2923 (2008) https://doi.org/10.1002/jps.21210

[42] Burdick JA, Prestwich GD. Hyaluronic acid hydrogels for biomedical applications. *Adv. Mater.*, **23**, H41–H56 (2011) https://doi.org/10.1002/adma.201003963

[43] Smart JD. The basics and underlying mechanisms of mucoadhesion. *Adv. Drug Deliv. Rev.*, **57**, 1556–1568 (2005) https://doi.org/10.1016/j.addr.2005.07.001

[44] Cheng L, Hill AF. Therapeutically harnessing extracellular vesicles. *Nat. Rev. Drug Discov.*, **21**, 379–399 (2022) https://doi.org/10.1038/s41573-022-00410-w

[45] Galsky MD, Hoimes CJ, Necchi A, Shore N, Witjes JA, Steinberg G, et al. Perioperative pembrolizumab therapy in muscle-invasive bladder cancer: Phase III KEYNOTE-866 and KEYNOTE-905/EV-303. *Future Oncol.*, **17**, 3137–3150 (2021) https://doi.org/10.2217/fon-2021-0273

[46] van der Heijden MS, Powles T, Gupta S, Loriot Y, Galsky MD, Valderrama BP, et al. Exploratory subgroup analyses of EV-302: A phase III global study to evaluate enfortumab vedotin in combination with pembrolizumab versus chemotherapy in previously untreated locally advanced or metastatic urothelial

carcinoma. *ESMO Open*, **10**, 105544 (2025) https://doi.org/10.1016/j.esmoop.2025.105544

[47] Liang CC, Park AY, Guan JL. In vitro scratch assay: A convenient and inexpensive method for analysis of cell migration *in vitro*. *Nat. Protoc.*, **2**, 329–333 (2007) https://doi.org/10.1038/nprot.2007.30

[48] Arnaoutova I, Kleinman HK. In vitro angiogenesis: Endothelial cell tube formation assay. *Nat. Protoc.*, **5**, 628–635 (2010) https://doi.org/10.1038/nprot.2010.6

[49] Goligher EC, Heath A, Harhay MO, Marshall JC, Thabane L, Rubenfeld GD, et al. Bayesian statistics for clinical research. *Lancet*, **404**, 1067–1076 (2024) https://doi.org/10.1016/S0140-6736(24)01295-9

[50] Ruxton GD. The unequal variance *t*-test is an underused alternative to Student's *t*-test and the Mann–Whitney *U* test. *Behav. Ecol.*, **19**, 690–693 (2008) https://doi.org/10.1093/beheco/arn020

[51] Pang R, Arbelaiz J, Pillow JW. Learning neural dynamics through instructive signals. *bioRxiv* (2025) https://doi.org/10.1101/2025.08.30.673300

[52] Calderon Martinez E, Ghattas Hasbun PE, Salolin Vargas VP, García-González OY, Fermin Madera MD, Rueda Capistrán DE, et al. A comprehensive guide to conduct a systematic review and meta-analysis in medical research. *Medicine (Baltimore).*, **104**, e41868 (2025) https://doi.org/10.1097/MD.0000000000041868